https://doi.org/10.31436/iiumej.v26i2.3556

ENHANCEMENT OF THE PHOTOCATALYTIC ACTIVITY OF MIL (53) METAL-ORGANIC FRAMEWORKS THROUGH THE ADDITION OF THE REDUCED GRAPHENE OXIDE FOR IMPROVING DEGRADATION OF ORGANIC DYE POLLUTANTS IN WATER TREATMENT APPLICATIONS

MUTTAQIN MUTTAQIN[1*], FANDRY HOSEA JABY[1], RIS KEVIN BRAMASTA[1], NONA MERRY MERPATI MITAN[1], YOSE FACHMI BUYS[2]

[1]Department of Chemistry, Universitas Pertamina, Jakarta, Indonesia
[2]Department of Mechanical Engineering, Universitas Pertamina, Jakarta, Indonesia

**Corresponding author: muttaqin@universitaspertamina.ac.id*

(Received: 29 December 2024; Accepted: 17 February 2025; Published online: 15 May 2025)

ABSTRACT: A simple nanocomposite consisting of MIL-53(Al) and reduced graphene oxide (rGO), denoted as MIL-53(Al)/rGO, was synthesized as a photocatalyst driven by sunlight and UV light to study the decomposition of methylene orange and methylene blue in aqueous solution. The MIL-53(Al)/rGO ultrafine particles were produced by an in situ method using the solvothermal technique. The nanocomposite was made with two different amounts of rGO, 2.5% and 5% by weight. Various tests, including XRD, N_2 adsorption-desorption isotherms, SEM, SEM-EDS, UV-Vis DRS (Diffuse Reflectance Spectroscopy), and FTIR, were performed on all photocatalyst variations to analyse their properties. Results from SEM and EDS showed the creation of small MIL-53(Al) particles measuring 10-20 μm and rGO spread evenly on the MIL-53(Al) surface, particularly in the 2.5% rGO sample. The photocatalytic effectiveness of the MIL-53(Al)/rGO nanocomposites was tested for degrading organic dyes (MO and MB) in water under both sunlight and UV light for 60- and 120-minute durations. The 2.5% rGO photocatalyst showed the highest performance, removing over 96% and 98% of the dyes after one hour of sunlight exposure for MB and MO, respectively. This demonstrates that the combined effect of MIL-53(Al) and rGO composite can be seen as an effective photocatalyst for breaking down reactive dyes, such as MO and MB, in water treatment applications.

ABSTRAK: Kajian ini adalah berkaitan nanokomposit sederhana daripada MIL-53(Al) dan grafit oksida yang tereduksi (rGO), atau MIL-53(Al)/rGO, berjaya disintesis sebagai fotopemangkin oleh cahaya matahari dan cahaya UV bagi mengkaji penguraian metil jingga (MO) dan metilena biru (MB) dalam larutan akueus. Zarah ultrahalus MIL-53(Al)/rGO dihasilkan melalui kaedah in situ menggunakan teknik solvotermal. Nanokomposit dibuat dengan dua jumlah rGO berat berbeza, 2.5 wt% dan 5 wt%. Pelbagai ujian termasuk XRD, N_2 penyerapan-nyahserapan isoterma (BET), SEM, SEM-EDS, UV-Vis DRS, dan FTIR telah dilakukan pada semua variasi fotopemangkin bagi mengkaji sifatnya. Dapatan kajian dari SEM dan EDS menunjukkan penciptaan zarah kecil MIL-53(Al) berukuran 10-20 μm dan rGO tersebar secara rata pada permukaan MIL-53(Al), terutamanya dalam sampel rGO 2.5%. Keberkesanan fotopemangkin nanokomposit MIL-53(Al)/rGO telah diuji bagi mengurai pewarna organik dalam air, di bawah kedua-dua cahaya matahari dan cahaya UV selama tempoh 60 dan 120 minit. Fotopemangkin rGO 2.5% menunjukkan prestasi tertinggi, dengan penyingkiran lebih dari 96% MB dan 98% MO, selepas pendedahan cahaya matahari selama satu jam. Ini menunjukkan, kesan gabungan komposit MIL-53(Al) dan rGO, boleh dilihat

sebagai fotopemangkin yang berkesan bagi memecahkan pewarna reaktif, seperti MO dan MB, dalam aplikasi rawatan air.

KEYWORDS: *Metal organic frameworks, Photocatalyst, Reduced graphene oxide, Organic Dye Pollutants, Degradation.*

1. INTRODUCTION

In the last decade, freshwater pollution by organic dyes has become a problem of concern for governments in every country. Industrial wastewater containing organic dyes is the most difficult waste to eliminate due to its high level of toxicity, difficult degradation process, high chromaticity content, and difficulty in removing the color [1]. Several methods have been introduced to remove organic dyes, such as physicochemical processes like adsorption, coagulation, and filtration. However, they include high costs, low efficiency, and the generation of large volumes of sludge that need further treatment [2][3]. Therefore, finding alternative technologies for removing toxic organic dyes in wastewater is essential. Advanced oxidation processes (AOPs) have emerged as a highly effective alternative for converting organic materials into simple mineral products [4][5]. Among AOPs, photocatalysis is seen as the most promising solution for sustainable energy conversion [6]. Researchers have focused on photocatalysis for its non-selectivity, efficiency in removing pollutants, and toxicity reduction. However, the complete degradation of organic dyes is time-consuming and less effective in some studies. Therefore, developing new and improved photocatalysts is necessary to address these issues. Materials that can be used as photocatalysts are semiconductors [7][8]. Semiconductors have proven to be promising materials as photocatalysts for degrading liquid organic waste [9]. In addition, photocatalysts have several advantages, such as low energy consumption, mild reaction conditions, reduction of secondary pollution, and so on, which have attracted wide attention domestically and internationally [10][11]. However, some semiconductor materials have disadvantages, such as being unresponsive to visible light (around 43% of the solar spectrum) and rapid recombination between electrons and holes [12][13]. Therefore, to overcome these limitations, the development of new photocatalysts with high efficiency, long-term stability, and the ability to harness visible light is necessary[14][15].

One of the materials that are included as semiconductors and receiving wide attention for application in the field of photocatalysis is metal-organic frameworks (MOFs) [16][17]. MOFs have a band gap that is not too large [18][19]. MOFs have the potential as semiconductor materials because they can transfer charge from ligands to metals (LMCT) or transfer charge from metals to ligands (MLCT). With this charge transfer ability, MOFs have photocatalytic capabilities to reduce hazardous materials [20]. One type of MOF with an interesting structure and widely studied is Hong Kong University of Science and Technology-1 (HKUST-1), a Cu-based MOF with benzene dicarboxylate organic ligands [21]. By adding graphene oxide (GO) to the HKUST-1 structure, the composition of these two materials has very good photocatalytic performance on organic dyes [22]. Furthermore, GO is a graphene-like material that has been functionalized with different oxygen-containing groups such as hydroxyl, carboxylic, carbonyl, and epoxide groups. Studies have shown that there are chemical bonds formed between MOF and substrates in composite materials [21]. Research indicates that the oxygen groups of GO are linked to the metal centres of the MOF in MOF/GO composites, leading to an enhanced ability to adsorb toxic gases such as NH_3, H_2S, and NO_2 [23][24]. But the use of nanocomposites combining MOF MIL-53 with Aluminium (Al) metal ion cluster and graphene-based materials like reduced graphene oxide (rGO) as highly effective photocatalysts has not been extensively studied until this point.

https://doi.org/10.31436/iiumej.v26i2.3556

In this study, we will perform and report the degradation process of organic dyes, methylene orange (MO) and methylene blue (MB), contaminating water using MOF MIL-53(Al) nanocomposite with rGO as co-doping. The photocatalyst synthesis method uses solvothermal techniques, while rGO is produced using the modified Marcano method [25]. MIL-53(Al) bandgap measurement shows great potential in photocatalysis because it has a band gap between 3.5 – 4.5 eV. The formation of nanocomposites between MOFs and rGO is expected to widen the range of absorption light and slow down the electron-hole recombination process of semiconductor materials based on MOFs.

2. METHODOLOGY

This section contains the materials we used, the synthesis method and process of the target materials, and various characterizations employed to determine the physical and chemical properties of the synthesized materials. The final part describes the testing methods used to evaluate the synthesized materials as photocatalysts.

2.1. Materials

The materials needed for this procedure are aluminium nitrate nonahydrate ($Al(NO_3)3{\cdot}9H_2O$, Merck KGaA), terephthalic acid or benzene-1,6-dicarboxylic acid (H_2BDC, 98%, Sigma Aldrich), graphite as a carbon source for GO/rGO synthesis, concentrated sulfuric acid (H_2SO_4, Mallinckrodt), phosphoric acid (H_3PO_4, Merck KGaA), 30% hydrogen peroxide (H_2O_2, Merck KGaA), potassium permanganate ($KMnO_4$, Sigma Aldrich 98%), N,N'-dimethylformamide (DMF, Merck KGaA), methanol (CH3OH, Merck KGaA), and distilled water. All materials are used directly without any purification steps.

2.2. Synthesis of Reduced Graphene Oxide (rGO)

The rGO synthesis followed previous work [25]. The process begins by preparing a 9:1 mixture of H_2SO_4/ H_3PO_4 (23 ml) and adding 1g of graphite powder. Afterward, 3g of $KMnO_4$ is slowly added to the solution, and the mixture temperature is maintained below 10°C during the addition process. The mixture is stirred for 40 minutes at 50°C and then diluted with deionized water. 30% hydrogen peroxide (H_2O_2) enhances the oxidation process. Adding H_2O_2 to the solution changes its colour to greenish yellow with bubbles indicating a high oxidation level. The solution is filtered and washed until the pH is near 7. The washing and filtration process of the rGO suspension was carried out by following the following steps: The rGO powder was dispersed in excess distilled water and stirred for 10 minutes using a magnetic stirrer at 300 rpm to neutralize the residual acid attached to the rGO. The rGO solid was then separated from the suspension solvent using a centrifuge, set at 5000 rpm for 10 minutes. This suspension formation and centrifugation process was repeated several times with excess distilled water until the pH of the rGO suspension approached 7. Finally, the product, rGO, is recovered and heated to 60°C overnight.

2.3. Synthesize nanocomposite Mil-53 (Al)/rGO

Synthesis of MIL-53 (Al)/rGO nanocomposites started by preparing the metal source from aluminium nitrate salt and the ligand source from terephthalic acid in a 1:1 molar ratio. Both materials are mixed and homogenized in DMF for 60 minutes under standard conditions. Afterwards, the rGO suspension was added in an amount of 2.5 to 5 % wt. of the total weight of the metal salt and ligand used and homogenized using a magnetic stirrer at around 400 rpm for 60 minutes. Then, the suspension is in a Durant bottle and is heated in an oven at 120°C for 72 hours to trigger the growth of MIL-53 (Al)/rGO crystals. After heating, the solid MIL-53

(Al)/rGO catalyst was recovered using a centrifugation technique at 5000 rpm for 10 minutes, then washed twice with methanol. The wet MIL-53 (Al)/rGO catalyst was dried at 80°C for 24 hours in the oven. Next, synthesized MIL-53 (Al)/GO is ground and sieved using a 200-mesh sieve. Finally, the catalyst was activated using a furnace at 160°C for 5 hours to produce dry nanocomposite MIL-53 (Al)/rGO.

2.4. Characterization

The samples were characterized using various analytical techniques. The infrared spectra were recorded using a NICOLET iS5 FT-IR spectrophotometer with ATR windows. Powder X-ray diffraction was performed with a Rigaku Miniflex 600 with a detector 1D−DteX/Ultra, Kβ filter. The XRD instrument uses a Cu-Kα radiation source. Furthermore, the morphological surface of the catalyst was examined using a Phenom Pro-X SEM. Finally, a Micrometrics TriStar II gas sorption and porosimeter device determined specific surface areas and porosity.

2.5. Photocatalytic Test

The photocatalyst testing of all photocatalyst materials was conducted by mixing 12 mg of the material with 20 mL of Methylene Blue (MB) or 20 mL of Methylene Orange (MO) at a concentration of 20 ppm in a reactor vessel. The mixture was stirred at 400 rpm using a magnetic stirrer for 60 and 120 minutes. The experimental setup for testing the photocatalyst material uses a glass reactor with the equipment arrangement as shown in Fig. 1. The photocatalyst performance tests were conducted under two types of light: UV light and sunlight. For UV light, the test was performed using a UV-A lamp with a wavelength range of 320-400 nm. For sunlight testing, the reactor containing the test solution was placed near a window to expose it to sunlight throughout the testing period. The cooling jacket was also filled with water, and the temperature was maintained at 30°C. This temperature was chosen as it is a moderate temperature typical for Jakarta and its surroundings.

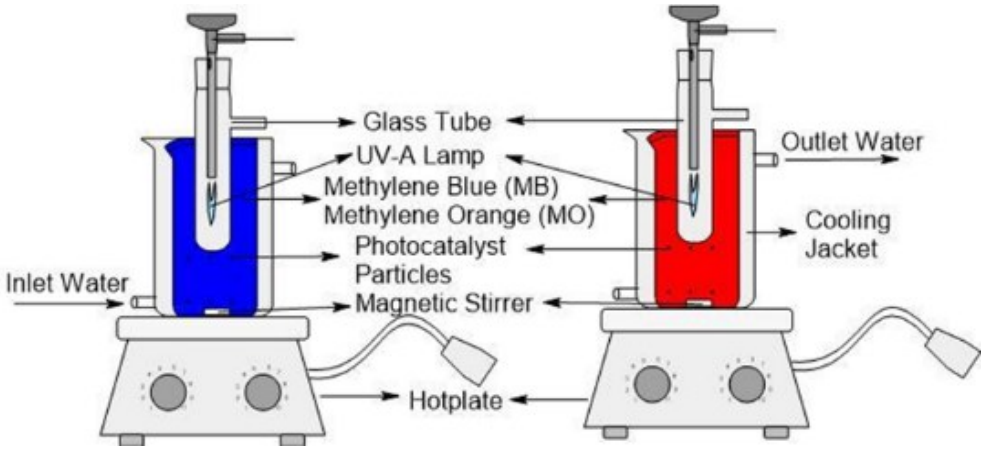

Figure 1. Experimental setup for organic dyes degradation using photocatalyst materials.

3. RESULTS AND DISCUSSION

3.1. FTIR SPECTRA

The interaction of aluminum (Al) ions and organic linker, H_2BDC, in the solvent, triggers the formation of covalent coordination bonds between metal ions and oxygen atoms derived from bidentate terephthalic acid [26]. As presented in Fig. 2, the wave numbers at 1417, 1511, and 1603 cm^{-1} correspond to a carbonyl (C=O) group and CO stretching in the C-OH

carboxylic group. Meanwhile, the wave numbers at 1001, 755, and 593 cm^{-1} indicate the C=O double bond in terephthalic acid, which interacts with metal ions and forms a single metal-O bond [27]. From FTIR data, we qualitatively assume that the target materials had been synthesized successfully.

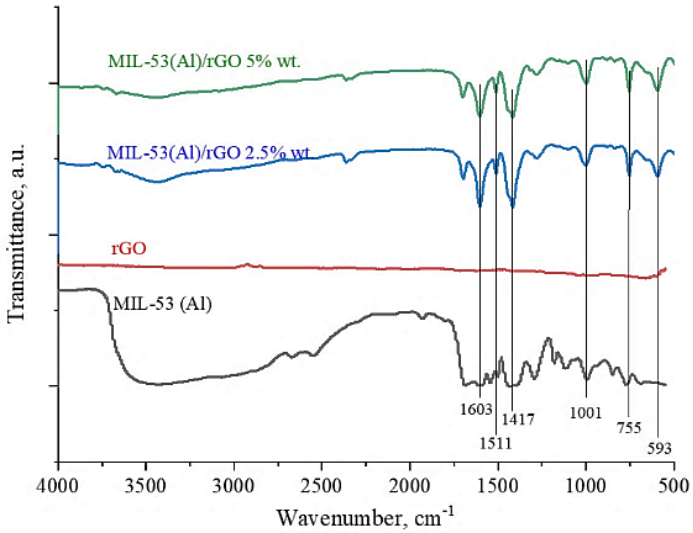

Figure 2. FTIR spectrums of MIL-53 (Al), rGO, MIL-53(Al)/rGO 2.5% wt., MIL-53(Al)/rGO 5% wt.

3.2. PHOTOCATALYST BANDGAP

The bandgap measurement of the photocatalytic materials was conducted using a UV-Vis DRS spectroscopy instrument. The sample reflects electromagnetic waves in the UV-Visible wavelength range in this measurement. Using the Tauc plot proposed by J. Tauc [28], the bandgap of a material can be calculated. The bandgap values for all photocatalyst variants are presented in the figure below.

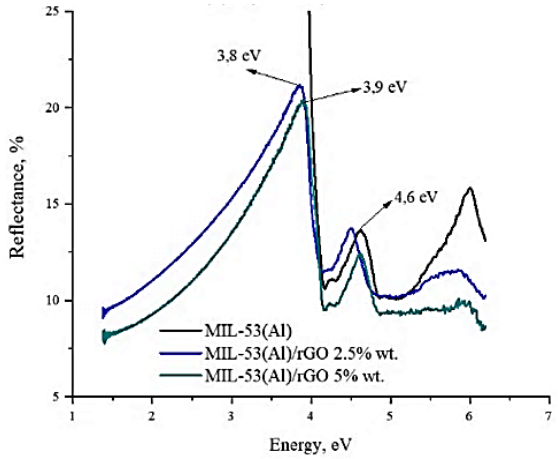

Figure 3. Bandgap measurement of photocatalyst materials.

Fig. 3 shows that the addition of 2.5% wt. rGO is effective in reducing the bandgap of the photocatalytic material. However, increasing the rGO ratio to 5% wt. does not further decrease the bandgap value. Instead, it remains the same or even slightly increases compared to the bandgap of the photocatalytic material without rGO. This phenomenon appears to be influenced by the decrease in the photocatalytic material's crystallinity and the increase in the size of the photocatalyst due to the increasing coverage by rGO.

https://doi.org/10.31436/iiumej.v26i2.3556

3.3. X-Rays Diffraction

XRD patterns of GO, rGO, and MIL-53(Al) and MIL-53(Al)/rGO composites are shown in Fig. 4. In the XRD pattern of the GO sample, the sharp intense peak at 2θ of 10° is assigned to the plane of [002] belonging to the GO layer [24]. In the XRD pattern of rGO, the sharp peak no longer exists but is replaced by a diffractogram representing material with amorphous properties. Interestingly, the diffractogram peak of the rGO sample appears at 2θ of 23°, a value similar to the 2θ peak of graphite [29]. In the XRD pattern of MIL-53 (Al), the strong peaks appear at 2θ of 9.13°, 10.05°, 15.36°, 18.26°, 20.91°, 25.45°, and 32.6° are several peaks characteristic of the MIL-53 (Al) phase, which match the peaks reported in the previous report [30]. In the XRD pattern of MIL-53(Al)/rGO, some diffraction peaks of MIL-53(Al) are still clearly visible, but these peaks appear at 2θ values that are either higher or lower. Furthermore, the amorphous profile, which belongs to rGO, does not appear due to mixing with the crystal structure of MIL-53(Al). This result indicates that MIL-53(Al) crystals may be well dispersed within the interlayers of GO/rGO sheets.

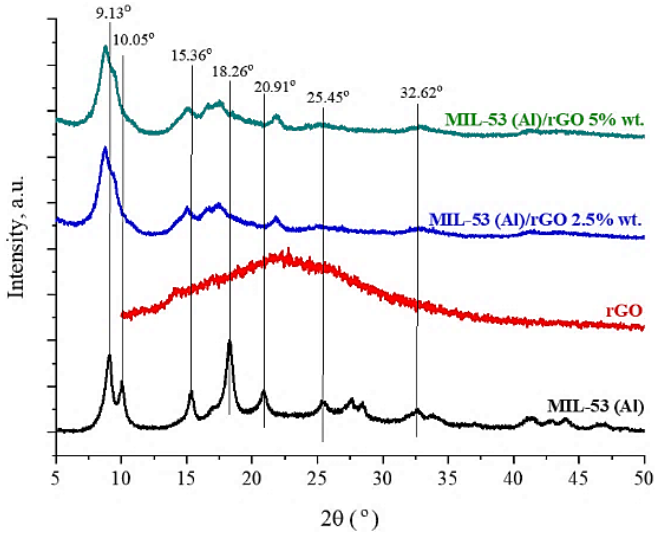

Figure 4. XRD patterns of: MIL-53 (Al), rGO, MIL-53(Al)/rGO 2.5% wt., MIL-53(Al)/rGO 5% wt.

3.4. SEM and SEM-EDS Analysis

The photocatalytic process is influenced by the physical characteristics of the catalyst, such as its active surface area and porosity. Smaller catalyst sizes result in a higher surface-to-mass ratio, reducing the distance electrons need to travel to the solid/solution interface and increasing efficiency. Therefore, our objective was to produce semiconductor nanocrystals to enhance light absorption. Scanning electron microscopy (SEM) images in Fig. 5 illustrate the morphology of MIL-53(Al), MIL-53(Al)/rGO 2.5% wt., MIL-53 (Al)/rGO 5% wt. From XRD testing results, the addition of rGO, both at 2.5% w.t and 5% w.t, did not significantly affect the crystal structure of MIL-53 (Al) because they have similar diffractogram profiles. This XRD result is supported by SEM profiles for MIL-53(Al)/rGO composites for all variants. The general SEM image of MIL-53(Al) appears as sub-micrometer particles with bar and flat cube surfaces and sharp or rounded edges [31]. The presence of GO/rGO surrounding the crystal structure of MIL-53(Al) did not alter its crystal structure dramatically, as seen in the following image.

https://doi.org/10.31436/iiumej.v26i2.3556

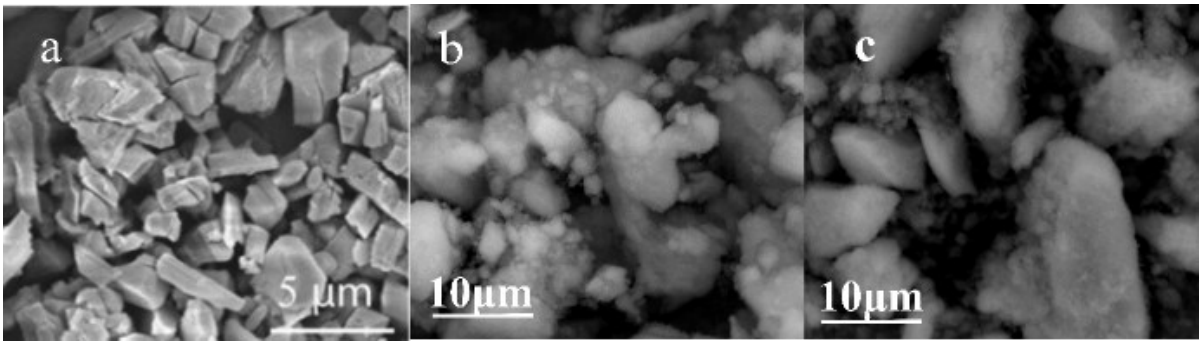

Figure 5. SEM profile for (a) MIL-53 (Al) [30], (b) MIL-53 (Al)/rGO 2.5% wt. (c) MIL-53/rGO 5% wt.

Fig. 5 shows that the addition of rGO ratio to the photocatalyst material leads to the coverage of the MIL-53 (Al) surface, resulting in larger crystallite sizes compared to the composite material with a lower rGO content and without rGO. As the crystallite size increases, the surface area decreases as shown in Table 1. The crystallite size measurements, presented in Table 1, show that the amount of rGO strongly influences the crystallite size added to the photocatalyst composition. As the rGO ratio increases, most MIL-53(Al) MOF surface interacts with rGO sheets. Since rGO still contains many oxygen-based functional groups, the interaction between crystallites becomes stronger due to hydrogen interaction, leading to an increase in crystallite size.

Table 1. The effect of rGO ratio on the crystallite size of the photocatalyst-composite material.

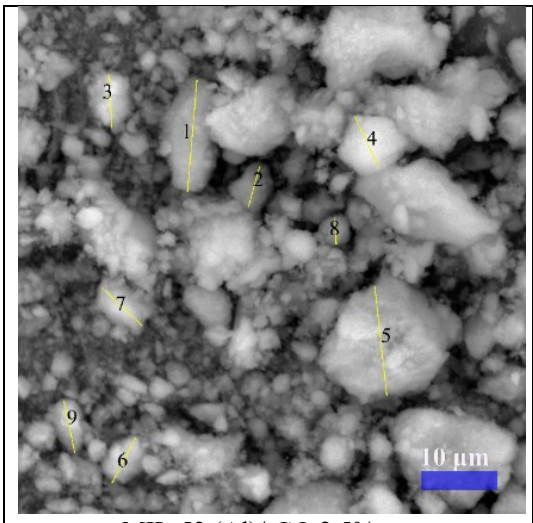

MIL-53 (Al)/rGO 2.5% wt.

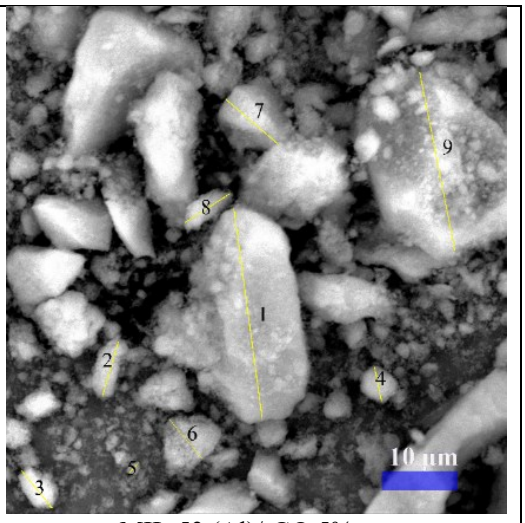

MIL-53 (Al)/rGO 5% wt.

No Particle	**Length of Particle (µm)**	**No Particle**	**Length of Particle (µm)**
1	10.15	1	28.32
2	4.63	2	8.04
3	5.92	3	6.05
4	6.27	4	4.74
5	13.47	5	1.95
6	4.49	6	9.22
7	5.52	7	9.51
8	3.03	8	7.46
9	7.29	9	25.08
Average	6.75	*Average*	11.15

https://doi.org/10.31436/iiumej.v26i2.3556

SEM-EDS analysis was performed to investigate the chemical composition of MIL-53(Al)/rGO. The EDX spectra (Fig. 6) of MIL-53(Al)/rGO showed that the amount of aluminium decreases with the increase in the rGO weight ratio. In Fig. 6, for MIL-53 (Al)/rGO 2.5% wt., the atomic percentage of Al is 10.04% when the rGO ratio is increased to 5% wt. (MIL-53 (Al)/rGO 5% wt.). The atomic percentage of Al decreases to 5.43%, nearly halving. The EDX spectra results qualitatively match the composition of the two variations of the photocatalyst composite materials well.

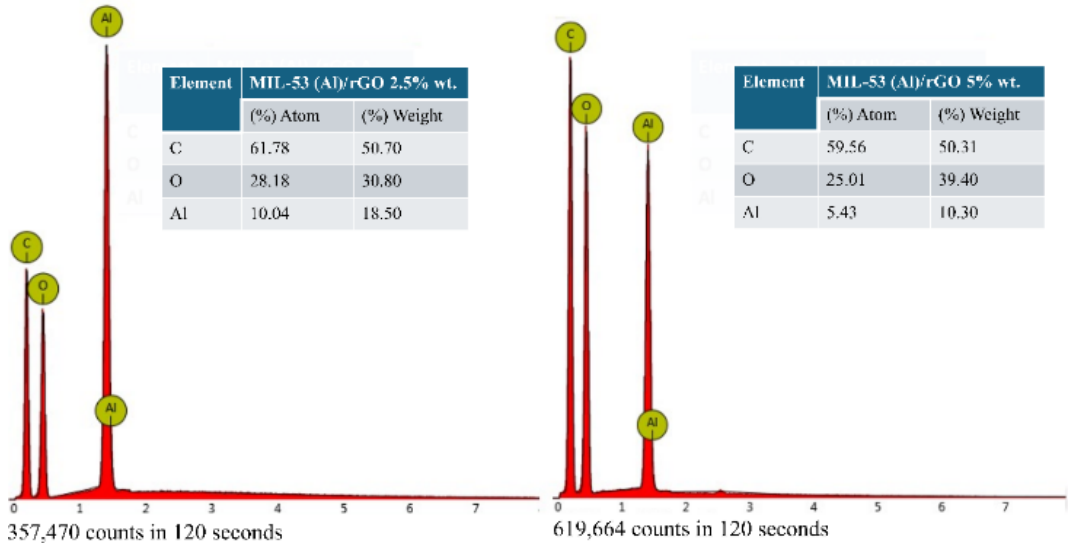

Figure 6. Elemental composition for each photocatalyst material

3.5. Nitrogen Isotherm adsorption

Fig. 7 shows that the isothermal curve of all photocatalyst samples shows type III based on the IUPAC classification.

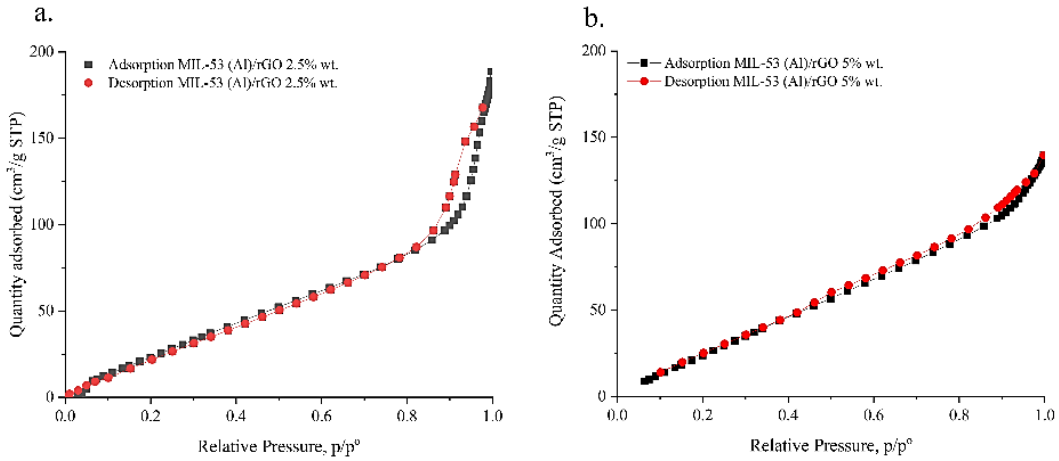

Figure 7. N_2 adsorption-desorption for synthesized MIL-53 (Al)/rGO. (a) 2.5% wt. rGO, (b) 5% wt. rGO.

The type-III adsorption isotherm, like the type-II isotherm, shows a general increase in adsorption with increasing pressure or concentration. As shown in Fig. 7, this rapid rise continues until the pressure is equal to the saturation pressure. At this point, adsorption is typically stable after relative pressure larger than 0.8, suggesting that the surface is saturated by adsorbate [32].

https://doi.org/10.31436/iiumej.v26i2.3556

3.6. Photocatalyst Performances

To evaluate the performance of the synthesized photocatalytic materials, tests were conducted to degrade two organic dyes, namely methylene blue (MB) 20 ppm and methyl orange (MO) 20 ppm, under UV and sunlight irradiation. The results of these tests are shown in Fig. 8.

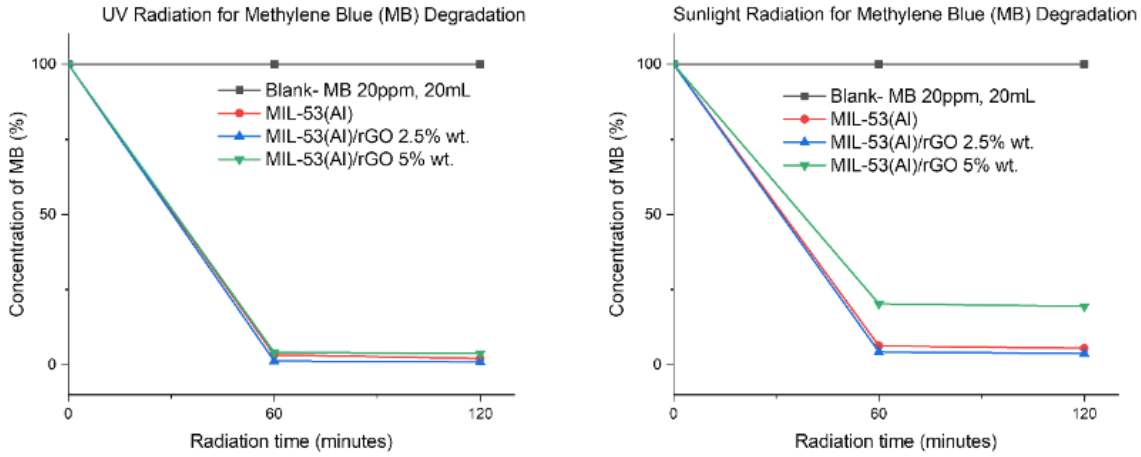

Figure 8. Photocatalyst performance under UV and Sunlight irradiation in 20 ppm MB solution.

Fig. 8 shows the performance of each photocatalyst material in degrading a 20 ppm MB test solution. Generally, all photocatalyst materials can degrade the test solution by more than 75% during the testing period. The MIL-53(Al)/rGO 2.5% wt. composition exhibits the best performance in degrading the test solution. Under sunlight, this composition can degrade the test solution by up to 97%, while under UV light, the test solution can be degraded by up to 99%. These results show that the MIL-53(Al) photocatalyst yields higher degradation of the test solution under sunlight than the MIL-53(Al)/rGO 5% wt. material shows slightly lower performance than the MIL-53(Al)/rGO 2.5% wt. composition. The poor photocatalytic performance of MIL-53(Al)/rGO 5% wt. under visible light, compared to other photocatalyst materials, is likely attributed to the larger crystallite size of this material resulting from the highest rGO ratio of 5%. As is well known, larger crystallite sizes can lead to a reduction in the number of active sites on the catalyst surfaces [33], facilitate faster recombination of electrons and holes [34], widen the bandgap [35], and enhance the stability of the photocatalyst material [36]. Ultimately, the increased crystallite size in the photocatalyst reduces its performance in degrading organic dye molecules.

A similar trend was observed for the methylene orange (MO) test solution. The photocatalyst with 2.5% wt rGO exhibited the best performance in degrading the 20 ppm MO solution within 60 and 120 minutes, under UV light and sunlight. The photocatalytic performance in the MO solution is presented in Fig. 9.

https://doi.org/10.31436/iiumej.v26i2.3556

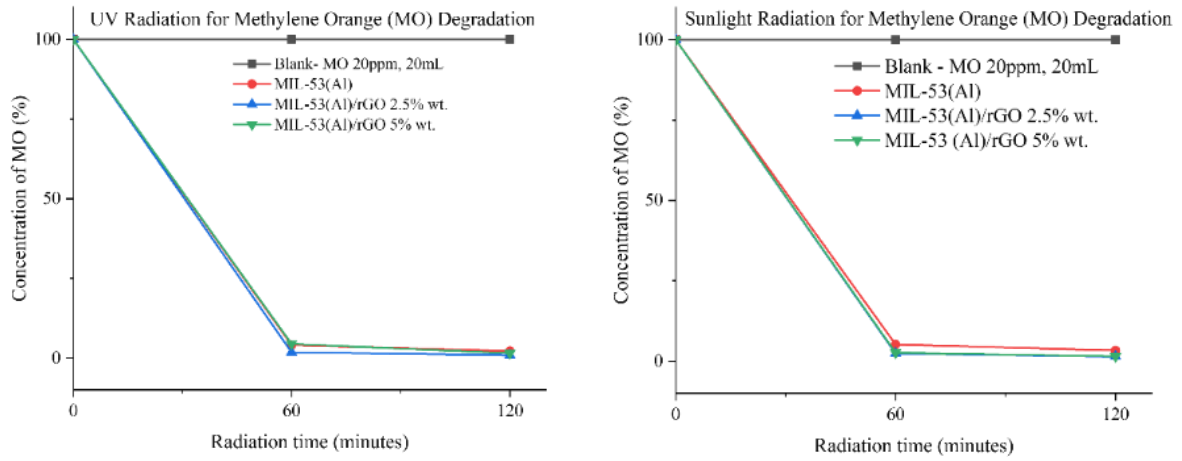

Figure 9. Photocatalyst performance under UV and Sunlight irradiation in 20 ppm MO solution.

3.7. General Mechanism of MIL-53(Al)/rGO Photocatalyst.

Methylene blue and methylene orange are synthetic dyes commonly used in various applications, including in the textile and pharmaceutical industries. Its decomposition under UV and sunlight irradiation in the presence of a photocatalyst involves photochemical reactions that lead to the breakdown of the dye molecules into smaller, non-toxic components. This process can be enhanced by using photocatalysts or other semiconductors, which facilitate photodegradation [24][37].

Here is an explanation of the mechanism of methylene blue and methylene orange decomposition using photocatalysts under UV and sunlight irradiation. UV-Irradiation: When UV light (typically in the range of 200-400 nm) is irradiated onto the photocatalyst, MIL-53 (Al), it excites the electrons (e^-) in the photocatalyst's valence band to the conduction band due to its relatively small bandgap. This creates electron-hole pairs, where the photogenerated electron (e^-) in the conduction band and hole (h^+) in the valence band are highly reactive. On the other hand, Sunlight Irradiation contains a broader spectrum, including visible light. To enhance the photocatalysis under sunlight, doping MIL-53(Al) with substances like rGO can allow the catalyst to absorb visible light and become activated under sunlight [9].

The electron-hole pairs generated in the photocatalyst due to UV or sunlight irradiation can migrate to the surface of the photocatalyst. The electron in the conduction band can participate in reducing species (such as oxygen molecules or water), while the hole in the valence band can oxidize other species (such as water or hydroxyl ions) [9]. Electron in the conduction band reacts with dissolved oxygen (O_2) in the solution to form superoxide anions ($O_2^{\bullet-}$), or they can reduce oxygen into hydrogen peroxide (H_2O_2)[38]. This leads to the formation of various reactive oxygen species (ROS), such as hydroxyl radicals (•OH) [38], [39], which are highly reactive and play a crucial role in the degradation of MB and MO.

$$O_2 + e^- \rightarrow O_2^{\bullet-} \text{ (superoxide anion)} \quad (1)$$

$$O_2^{\bullet-} + H_2O \rightarrow H_2O_2 + OH^- \text{ (hydrogen peroxide and hydroxyl ion)} \quad (2)$$

On the other side, the hole in the Valence Band reacts with water (H_2O) or hydroxide ions (OH^-) on the surface of the photocatalyst to generate hydroxyl radicals (•OH), which are strong oxidants capable of attacking and degrading MB molecules.

$$H_2O + h^+ \rightarrow \bullet OH + H^+ \text{ (formation of hydroxyl radicals)} \quad (3)$$

https://doi.org/10.31436/iiumej.v26i2.3556

$$OH^- + h^+ \rightarrow \bullet OH \text{ (formation of hydroxyl radicals)} \quad (4)$$

The reactive oxygen species (ROS), such as hydroxyl radicals (•OH), superoxide anions ($O_2\bullet^-$), and hydrogen peroxide (H_2O_2), are highly reactive and can attack the methylene blue and methylene orange molecules. The degradation of MB and MO primarily involves the following steps. The ROS oxidizes the aromatic structure of MB and MO, breaking the chemical bonds in the dye and leading to the formation of smaller, less complex molecules, eventually mineralizing to carbon dioxide (CO_2) and water (H_2O)[39]. The next step is demethylation and decolorization. The methyl groups on the MB and MO molecules may be oxidized or broken down, leading to a loss of color. The photodegradation process of MO and MB is presented schematically in Fig. 10.

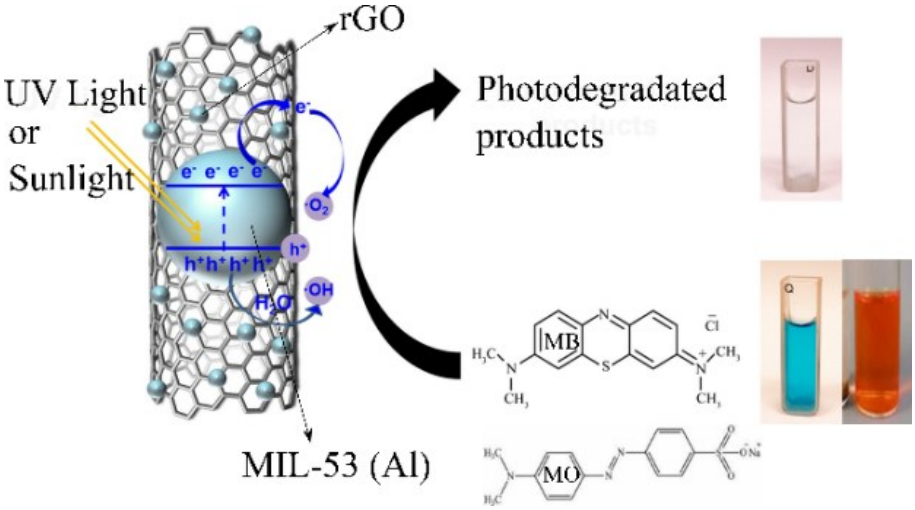

Figure 10. The process of photodegradation of MO and MB using MIL-53 (Al)/rGO

The breakdown of the chromophore (the part of the molecule responsible for its color) leads to the decolorization of MB and MO. From our experimental data, the process of dye decomposition is more efficient under UV light because of the high energy available to activate the photocatalyst. Under sunlight, the process can still occur, but it may be slower or require modified photocatalysts that can absorb visible light. Furthermore, factors like temperature and pH can improve this mechanism, and the presence of additional substances like co-catalysts or sacrificial agents can enhance the efficiency of MB and MO degradation.

4. CONCLUSION

The photocatalyst materials were successfully synthesized via the solvothermal method, producing three variants: MIL-53(Al), MIL-53(Al)/rGO (2.5 wt.%), and MIL-53(Al)/rGO (5 wt.%). FTIR analysis confirmed their composition, with characteristic absorption peaks at 1417 cm^{-1}, 1511 cm^{-1}, and 1603 cm^{-1}, indicating the presence of carbonyl and carboxyl functional groups. The IR spectra at wave numbers 1001, 755, and 593 cm^{-1} indicate the vibrational interaction between metal ions and oxygen bonds. XRD characterization confirmed the crystalline structure of the materials. MIL-53(Al) showed distinct diffraction peaks consistent with reported data, while rGO exhibited an amorphous peak at $2\theta = 23°$, characteristic of graphite. Additionally, combining MIL-53(Al) with rGO caused a shift in diffraction peaks at 2θ and peak broadening due to the amorphous nature of rGO. However, both materials retained their characteristic peaks, confirming successful synthesis. The incorporation of rGO

influenced the photocatalyst's morphology, with higher rGO content nearly doubling its size, decreasing surface area, and affecting dye degradation efficiency. N_2 adsorption-desorption data revealed that larger particles had reduced gas adsorption capacity, which impacted their photocatalytic activity. Additionally, introducing a small amount of rGO reduced the bandgap from ~4 eV to 3.8 eV, though further rGO addition had no significant effect. Photocatalytic tests showed that MIL-53(Al)/rGO (2.5 wt.%) achieved the highest degradation efficiency, breaking down MB and MO dyes almost completely (~100%) within 120 minutes under both UV and sunlight irradiation.

ACKNOWLEDGEMENT

This work was supported by the Early-Career Researcher (Penelitian Dosen Pemula) Grant Scheme 2024, from the Ministry of Education, Culture, Research, and Technology of the Republic of Indonesia, contract number 105/E5/PG.02.00.PL/2024.

REFERENCES

[1] L. Liu, Z. Chen, J. Zhang, D. Shan, Y. Wu, L. Bai, B. Wang. Treatment of industrial dye wastewater and pharmaceutical residue wastewater by advanced oxidation processes and its combination with nanocatalysts: A review. *J. Water Process Eng.* 2021; 42(22): 102122. doi: 10.1016/j.jwpe.2021.102122.

[2] S. Jorfi, S. Pourfadakari, and B. Kakavandi. A new approach in sono-photocatalytic degradation of recalcitrant textile wastewater using MgO@Zeolite nanostructure under UVA irradiation. Chem. Eng. J. 2018 Jul; 343: 95–107. doi: 10.1016/j.cej.2018.02.067.

[3] M. S. Jami, M. Mel, A. R. M. Ariff, Q. M. Abdulazeez. Investigation of bioflocculant as dewatering aid in sludge treatment. IIUM Eng. J. 2018; 19(1): 15–23. doi: 10.31436/iiumej.v19i1.735.

[4] J. Wang, S. Wang. Reactive species in advanced oxidation processes: Formation, identification and reaction mechanism. Chem. Eng. J.2020; 401:126158. doi: 10.1016/j.cej.2020.126158.

[5] G. I. Lupu, C. Orbeci, L. Bobirică, C. Bobirică, L. F. Pascu. Key Principles of Advanced Oxidation Processes: A Systematic Analysis of Current and Future Perspectives of the Removal of Antibiotics from Wastewater. Catalysts. 2023; 13(9). doi: 10.3390/catal13091280.

[6] S. A. Younis, E. E. Kwon, M. Qasim, K-H. Kim, T. Kim, D. K, X. Dou, I. Ali. Metal-organic framework as a photocatalyst: Progress in modulation strategies and environmental/energy applications. Progress in Energy and Combustion Science. 2020 Nov. 01;81. doi: 10.1016/j.pecs.2020.100870.

[7] F. Zhang, X. Wang, H. Liu, C. Liu, Y. Wan, Y. Long, Z. Cai. Recent advances and applications of semiconductor photocatalytic technology. Appl. Sci. 2019; 9(12). doi: 10.3390/app9122489.

[8] M. Nemiwal, V. Subbaramaiah, T. C. Zhang, D. Kumar. Recent advances in visible-light-driven carbon dioxide reduction by metal-organic frameworks. Sci. Total Environ. 2021; 762: 144101. doi: 10.1016/j.scitotenv.2020.144101.

[9] Y. Chen, B. Y. Zhai, Y. N. Liang, Y. Li. Hybrid photocatalysts using semiconductor/MOF/graphene oxide for superior photodegradation of organic pollutants under visible light. Mater. Sci. Semicond. Process. 2020 Mar;107. doi: 10.1016/j.mssp.2019.104838.

[10] M. A. Hassaan, M. A. El-Nemr, M. R. Elkatory, S. Ragab, V. C. Niculescu, A. El Nemr. Principles of Photocatalysts and Their Different Applications: A Review. 2023; 381(6). Springer International Publishing.

[11] N. Mohammed, P. Palaniandy, F. Shaik, H. Mewada. Experimental and Computational Analysis

for Optimization of Seawater Biodegradability Using Photo Catalysis. IIUM Eng. J. 2023;24(2):11–33. doi: 10.31436/iiumej.v24i2.2650.

[12] N. Sun, X. Si, L. He, J. Zhang, Y. Sun. Strategies for enhancing the photocatalytic activity of semiconductors. Int. J. Hydrogen Energy. 2024 Mar; 58: 1249–1265. doi: 10.1016/J.IJHYDENE.2024.01.319.

[13] C. B. Anucha, I. Altin, E. Bacaksiz, V. N. Stathopoulos. Titanium dioxide (TiO_2)-based photocatalyst materials activity enhancement for contaminants of emerging concern (CECs) degradation: In the light of modification strategies. Chem. Eng. J. Adv. 2022 Feb; 10:100262. doi: 10.1016/j.ceja.2022.100262.

[14] V. García-Salcido, P. Mercado-Oliva, J. L. Guzmán-Mar, B. I. Kharisov, L. Hinojosa-Reyes. MOF-based composites for visible-light-driven heterogeneous photocatalysis: Synthesis, characterization and environmental application studies. J. Solid State Chem.2022 Mar; 307: 122801. doi: 10.1016/J.JSSC.2021.122801.

[15] Y. Bai, S. Zhang, S. Feng, M. Zhu, S. Ma. The first ternary Nd-MOF/GO/Fe3O4nanocomposite exhibiting an excellent photocatalytic performance for dye degradation. Dalt. Trans. 2020 Aug; 49(31): 10745–10754. doi: 10.1039/d0dt01648a.

[16] E. Özcan, Z. Mermer, Y. Zorlu. Metal-organic frameworks as photocatalysts in energetic and environmental applications. Turkish J. Chem. 2023;47(5): 1018–1052. doi: 10.55730/1300-0527.3592.

[17] W. Ma, L. Yu, P. Kang, Z. Chu, Y. Li. Modifications and Applications of Metal-Organic-Framework-Based Materials for Photocatalysis. Molecules. 2024; 29(24). doi: 10.3390/molecules29245834.

[18] A. Sugie, K. Nakano, K. Tajima, I. Osaka, H. Yoshida. Dependence of Exciton Binding Energy on Bandgap of Organic Semiconductors. J. Phys. Chem. Lett. 2023;14(50):11412–11420. doi: 10.1021/acs.jpclett.3c02863.

[19] P. H. M. Andrade, C. Volkringer, T. Loiseau, A. Tejeda, M. Hureau, A. Moissette. Band gap analysis in MOF materials: Distinguishing direct and indirect transitions using UV–vis spectroscopy. Appl. Mater. Today. 2024 Jan; 37: 102094. doi: 10.1016/j.apmt.2024.102094.

[20] S. Javanbakht, M. Pooresmaeil, H. Hashemi, H. Namazi. Carboxymethylcellulose capsulated Cu-based metal-organic framework-drug nanohybrid as a pH-sensitive nanocomposite for ibuprofen oral delivery. Int. J. Biol. Macromol. 2018 Nov;119: 588–596. doi: 10.1016/j.ijbiomac.2018.07.181.

[21] M. Muttaqin, F. I. Hidayat. A modest method of synthesis Cu- based metal-organic frameworks using benzene dicarbocxylate as a ligan for promising candidate of flue gas CO_2 adsorption. J. Nat. 2021 Oct;21(3): 128–134. doi: 10.24815/jn.v21i3.20035.

[22] J. Zhang, C. Su, X. Xie, P. Liu, M. E. Huq. Enhanced visible light photocatalytic degradation of dyes in aqueous solution activated by HKUST-1: performance and mechanism. RSC Adv. 2020;10(61):37028–37034. doi: 10.1039/d0ra05275b.

[23] Y. Chen, B. Y. Zhai, Y. N. Liang, Y. Li. Hybrid photocatalysts using semiconductor/MOF/graphene oxide for superior photodegradation of organic pollutants under visible light. Mater. Sci. Semicond. Process. 2020 Mar;107: 104838. doi: 10.1016/J.MSSP.2019.104838.

[24] H. T. Vu, L. T. Tran, G. H. Le, Q. K. Nguyen, T. M. Vu, T. A. Vu. Synthesis and application of novel Fe-MIL-53/GO nanocomposite for photocatalytic degradation of reactive dye from aqueous solution. Vietnam J. Chem. 2019 Dec;57(6): 681–685. doi: 10.1002/vjch.201900055.

[25] M. Husnah, H. A. Fakhri, F. Rohman, A. H. Aimon, F. Iskandar. A modified Marcano method for improving electrical properties of reduced graphene oxide (rGO). Mater. Res. Express. 2017

Jun;4(6). doi: 10.1088/2053-1591/aa707f.

[26] C. G. Carson, K. Hardcastle, J. Schwartz, X. Liu, C. Hoffmann, R. A. Gerhardt, R. Tannenbaum. Synthesis and structure characterization of copper terephthalate metal-organic frameworks. Eur. J. Inorg. Chem. 2029;(16): 2338–2343. doi: 10.1002/ejic.200801224.

[27] C. G. Carson, G. Brunnello, S. G. Lee, S. S. Jang, R. A. Gerhardt, R. Tannenbaum. Structure solution from powder diffraction of copper 1,4- benzenedicarboxylate. Eur. J. Inorg. Chem. 2014;(12): 2140–2145. doi: 10.1002/ejic.201301543.

[28] P. Makuła, M. Pacia, W. Macyk. How To Correctly Determine the Band Gap Energy of Modified Semiconductor Photocatalysts Based on UV-Vis Spectra. J. Phys. Chem. Lett. 2018; 9(23): 6814–6817. doi: 10.1021/acs.jpclett.8b02892.

[29] S. Mundinamani. Large Area, Multilayer Graphene Films as a Flexible Electronic Material. ACS Omega. 2020 Jul;5(28): 17479–17485. doi: 10.1021/acsomega.0c01982.

[30] T. Loiseau, C. Serre, C. Huguenard, G. Fink, F. Taulelle, M. Henry, T. Bataille, G. Ferey. A Rationale for the Large Breathing of the Porous Aluminum Terephthalate (MIL-53) Upon Hydration. Chem. - A Eur. J. 2004 Apr;10(6): 1373–1382. doi: 10.1002/chem.200305413.

[31] X. Qian, B Yadian, R. Wu, Y Long, K. Zhou, B. Zhu, Y. Huang. Structure stability of metal-organic framework MIL-53 (Al) in aqueous solutions. Int. J. Hydrogen Energy. 2013 Dec;38(36): 16710–16715. doi: 10.1016/j.ijhydene.2013.07.054.

[32] M. Burhan, M. W. Shahzad, K. C. Ng. Energy distribution function based universal adsorption isotherm model for all types of isotherm. Int. J. Low-Carbon Technol. 2018;13(3):292–297. doi: 10.1093/IJLCT/CTY031.

[33] J. Gorimbo, R. Chikati, P. Khangale, I. N. Beas, L. L. Mguni, D. Nkazi. Debunking the impact of crystallite/particle size in cobalt-based Fischer-Tropsch synthesis. Chemical Engineering Communications. 2024;211(8):1262–1287. Taylor and Francis Ltd. doi: 10.1080/00986445.2024.2341263.

[34] R. Chuliá-Jordán, E. J. Juarez-Perez. Short Photoluminescence Lifetimes Linked to Crystallite Dimensions, Connectivity, and Perovskite Crystal Phases. J. Phys. Chem. C. 2022 Feb;126(7): 3466–3474. doi: 10.1021/acs.jpcc.1c08867.

[35] B. M. John, S. W. Mugo, J. M. Ngaruiya. Dependence of Optical Band Gap on Crystallite Size of TiO_2 Thin Films Prepared Using Sol Gel Process. European Journal of Material Science.2021; 8(1): 1-12. doi: 10.2139/ssrn.3819728.

[36] A. B. D. Nandiyanto, R. Zaen, R. Oktiani. Correlation between crystallite size and photocatalytic performance of micrometer-sized monoclinic WO3 particles. Arab. J. Chem. 2020 Jan;13(1): 1283–1296. doi: 10.1016/j.arabjc.2017.10.010.

[37] A. Fawzy, H. Mahanna, M. Mossad. Effective photocatalytic degradation of amoxicillin using MIL-53(Al)/ZnO composite. Environ. Sci. Pollut. Res. 2022 Sep;29(45): 68532–68546. doi: 10.1007/s11356-022-20527-0.

[38] B. Wang, L. Shen, J. Xu, Z. Yang, Y. Chen, S. Chen, B. Li, C. Chen, H. Lin. Graphene oxide-assisted dispersion and assembly of photocatalytic self-cleaning MOF membrane for enhanced water purification. Sep. Purif. Technol. 2025 Apr;356:129928. doi: 10.1016/J.SEPPUR.2024.129928.

[39] Z. U. Zango, K. Jumbri, N. S. Sambudi, A. Ramli, N. H. H. Abu Bakar, B. Saad, M. N. H. Rozani, H. A. Isiyaka, A. H. Jagaba, O. Aldaghri, A. Sulieman. A critical review on metal-organic frameworks and their composites as advanced materials for adsorption and photocatalytic degradation of emerging organic pollutants from wastewater. Polymers. 2020 Nov;12(11):1–42. MDPI AG. doi: 10.3390/polym12112648.